2013 Eighth International Conference and Exhibition on Ecological Vehicles and Renewable Energies (EVER)

InMotion: Hybrid Race Car, beating F1 at LeMans

J. Jacob*, J.A. Colin*, H. Montemayor*, D. Sepac*, H.D. Trinh*,
S.F. Voorderhake*, P. Zidkova*, J.J.H. Paulides†, A. Borisavljevic†,
and E.A. Lomonova†

*PDEng Automotive Systems Design, Stan Ackermans Institute,
Eindhoven University of Technology. Eindhoven, The Netherlands.
†Electromechanics and Power Electronics group, Department of Electrical Engineering,
Eindhoven University of Technology. Eindhoven, The Netherlands.

***Abstract*—This paper presents the design of a hybrid electric powertrain for the InMotion IM01 race car. InMotion is a multidisciplinary project group of experienced master students, PhD students, and professors from Eindhoven University of Technology (TU/e). The authors of this paper were involved in the project to develop a suitable powertrain architecture for use in the IM01 series hybrid race car. The most important requirements were to achieve a lap time of below 2 min 45 s on the Circuit de la Sarthe, and to have a durability, efficiency, cornering speed, and acceleration that exceeds Formula 1 race cars. Data provided from InMotion included design restrictions, a simplified drive cycle, and technical data of some components. This data was analyzed and the required powertrain component sizes were determined. A detailed drive cycle calculation and sensitivity analysis were introduced to find the variables that significantly influence the lap time. The powertrain was modeled using the backwards approach and an energy management strategy was designed with the objective of minimizing fuel consumption. Finally, five different powertrain configurations were presented, and several tradeoffs between lap time and different parameters were discussed. The results showed that the fastest achievable lap time using the proposed configurations was 3 min 9 s. It was concluded that several car and component parameters have to be improved to decrease this lap time to the required 2 min 45 s. Recommendations for future work to achieve this were addressed.**

***Index Terms*—Series hybrid electric race car, powertrain design, race car dynamics, energy management strategy.**

I. Introduction

Race cars are an excellent showcase for new technologies from the different areas of automotive systems. The InMotion project group utilizes the state-of-the-art research in the automotive domain that is being carried out at the Eindhoven University of Technology for the design of a high tech and innovative race car. The aim for this race car will be able to drive autonomously around the race track Circuit de la Sarthe in France, with a lap time faster than a Formula 1 car. The designed vehicle will be a hybrid electric vehicle with the implementation of many advanced innovations.

Nowadays, hybrid powertrains have indeed become a topic of interest for racing vehicles. Formula 1 (2012 season) incorporates a Kinetic Energy Recovery System (KERS), which can store up to 400 kJ with a maximum power of 60 kW. One objective of introducing the KERS system is to promote the development of environmentally friendly and road car relevant technologies in Formula 1 racing [1]. Audi incorporates a flywheel accumulator system in the R-18 e-tron Quattro racing vehicle for the 24 hours of Le Mans race. This system can recover up to 500 kJ of energy while braking [2]. Lambert et al. [3] proposed a methodology for the development of a hybrid electric racing car with the aim of increasing the maximum acceleration. It was found that different parallel architectures can increase acceleration performance with the use of an electric machine and energy storage system. Mappelli et al. [4] introduced an energy management strategy for a plug-in parallel hybrid race car to reduce the overall energy consumption for competing in the Federation Internationale de L'automobile (FIA) alternative energy car race. Simulation results show that it is possible to reduce fuel consumption over a complete race by about 5%. Sibley and Emadi [5] introduced a control analysis for hybrid electric vehicles designed for high performance applications. It was concluded that the trade-off between efficiency and performance can be addressed by adding constraints on the driver's demand for quick acceleration and by using neural networks for optimization of the energy flow in the powertrain. Benson et al. [6] explored the potential of a series hybrid gas electric propulsion system for a race vehicle designed for Formula SAE (FSAE). The hybrid configuration includes ultracapacitors, a 206 cm^3 engine, a permanent magnet brushed generator, an induction motor, and a fixed-ratio gearbox. It was concluded that the hybrid powertrain can offer significant advantages in terms of acceleration. High torque densities are a key requirement in traction machines. Using a multiple air gap design, as proposed in [7], up to 60% higher torque density relative to single air gap machines can be achieved.

At the start of the InMotion race car design project, the authors of this paper temporarily became part of the project team, and their task was to design a powertrain system. InMotion had the following goals with respect to the powertrain:

- The vehicle should have a high efficiency, which should be achieved by designing a hybrid electric powertrain that is controlled by an optimized Energy Managment Strategy (EMS).
- The hybrid powertrain should have a series hybrid topology. This is due to relative mechanical simplicity of the

978-1-4673-5271-0/13/$31.00 ©2013 IEEE

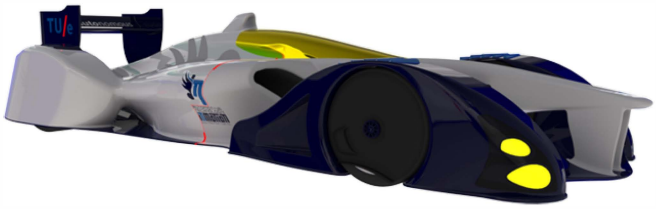

Fig. 1. Iso view of InMotion IM01

topology, when compared to other hybrid topologies.
- The performance in terms of cornering speed and acceleration should exceed that of a Formula 1 race car.
- The vehicle should have a higher durability than a Formula 1 car, i.e., be able to complete the 24 hours of Le Mans race.

Background research was done on hybrid vehicle topologies and technologies. Based on the goals of InMotion, the steps to be taken in designing the powertrain were defined.

A. Background

Hybrid electric vehicles make use of the best characteristics of engine, motor, energy storage and other complementary components. There are two main types of powertrain topologies: series and parallel. The series topology has the advantages of a simpler control strategy, mechanical simplicity and the possibility to use a lightweight high speed engine. The disadvantages include that when energy is being provided from the engine, the energy has to pass through both generator and motor, which increases the losses compared to the parallel topology. Moreover, in case there is no energy storage device, the motor, engine and generators each have to be fully sized to meet the required power demand. This results in a relatively heavy powertrain, when compared to a conventional one. For the parallel topology, the engine size can be reduced because the engine can drive the wheels directly in combination with the electric motors. Furthermore, it is possible to use three driving modes which are engine only, motor only, or a combination of engine and motor. However, directly connecting the engine with the wheels requires a low speed engine or large gear ratios. Together with the more complex transmission to be able to switch between the modes of operation, this makes for larger mechanical losses and a more complex control strategy. In both mentioned architectures, energy storage plays a very important role. Among the most known devices are battery, ultracapacitor, flywheel, fuel cell and hydrogen supply.

The racing circuit consists mainly of sections where brisk acceleration and heavy braking are needed. On one hand, this implies a large power demand from the powertrain. On the other hand, this means that there is a possibility to regenerate an enormous amount of energy by regenerative braking. Modern batteries, especially those with li-ion phosphate technology, are high in energy content. However, they are limited in terms of power and frequency of charging and discharging. In contrast, ultracapacitors have very high charging and discharging rates, but they are low in energy content.

Given this background on hybrid electric vehicles, a sequence of design steps had to be defined, which would help in designing a hybrid electric powertrain with the right technology choices and component sizings that would meet InMotion's requirements.

B. The design steps

To succesfully design a powertrain that can fulfill the needs of InMotion, five main steps were performed:

1) Definition of requirements: basic performance requirements were defined based on research on the capabilities of Formula 1 race cars. In order to limit the design space and account for the limitation of the race car, some constraints were imposed on the design.
2) Drive cycle generation: a drive cycle was created using these performance requirements as well as other necessary inputs such as the track layout of Circuit de la Sarthe, the drag coefficient, the tire specifications, and the mass of the vehicle.
3) Selection of technology: the drive cycle was used to model the power requirements from the powertrain components of the series-hybrid topology, which acted as input to identify what technology is more suitable for the race car (i.e., which motors, generators, converters, and energy storage technology to use).
4) Lap time sensitivity analysis: the impact of certain design decisions on lap time was determined by the lap time sensitivity analysis. This analysis made it possible to further narrow down the design space.
5) Modeling and optimization: the design involved building the energy management strategy that optimizes the energy flow throughout the powertrain. This gave an estimation of how much fuel is consumed in the drive cycle with the components selected in the previous steps. This final step also involved comparing the fuel consumption of the energy management strategy for different sizes of the components used in the powertrain (number of motors used, size of the storage, etc). The comparison of these different results showed the advantages and disadvantages of each configuration for the powertrain.

Sections II to VI describe each step in detail. Finally, conclusions are made in Section VII.

II. Definition of Requirements

In this step of the design, performance requirements were defined based on the goals of InMotion. These requirements were derived based on research into Formula 1 race cars. In addition to these requirements, some design constraints were imposed so as to limit the design space.

TABLE I. 2004 F1 acceleration profile as given by InMotion

Speed [km/h]	0	25	100	200	250	300	350
Time [s]	0	0.42	1.70	3.80	5.50	8.60	13.6

A. Performance requirements

The goal of InMotion is to show that Formula 1 technology, although very advanced, does not represent state-of-the-art research due to rule restrictions. It is therefore very important to beat a Formula 1 race car in every way possible. For this reason it was decided that the InMotion race car should accelerate faster than a Formula 1 race car, have a higher top speed, and hence have a shorter lap time on the Le Mans circuit. The required lap time was defined to be 2 min 45 s. This is a 10 second improvement on the estimated Formula 1 lap time on the Circuit de la Sarthe of 2 min 55 s [10]. For the top speed, a speed of 350 km/h is used and the acceleration profile of the 2004 F1 was considered, since more recent data was not available. This acceleration profile is shown in Table I.

B. Design constraints

InMotion imposed certain constraints on the powertrain design, which were as follows:

- Maximum weight for the energy storage is 250 kg for a single energy storage type and 350 kg for two storage types.
- The energy storage volume is limited to two times 0.072 m^3 with a base of 0.36 m^2.
- The DC-link voltage is limited to 1 kV.
- no plug-in capability.

III. Drive Cycle Generation

Initially, the drive cycle is calculated to describe the velocity of the race car at each location on the track. To generate this drive cycle, the track layout was extracted as described in Section III-A. The tire friction coefficients, which represent an important limitation of the maximum speed achievable in the drivecycle, were estimated as shown in Section III-B. After that the velocity at each point was be determined. This velocity is calculated in three steps. First, the maximum velocity due to the limitation on the lateral force that can be generated by the tires, was calculated (i.e. the velocity at which the lateral force equals to the maximum that the tires can handle, this is described in Section III-C). Second, the limited braking power of the race car was taken into account (Section III-D). Finally, the acceleration performance was used (Section III-E).

The model used for the drive cycle was based on a bicycle model. Although the bicycle model has the disadvantage that it does not compute the lateral load transfers (body roll is not considered), its calculation time is very short compared to a full vehicle model. Besides, there were not enough data on vehicle parameters to build a full vehicle model. The speed was calculated first as a function of position, and then it was expressed as a function of time. In this way, it was possible to compare the calculated drive cycle to the drive cycle from the Audi R18 e-tron quattro race car [11].

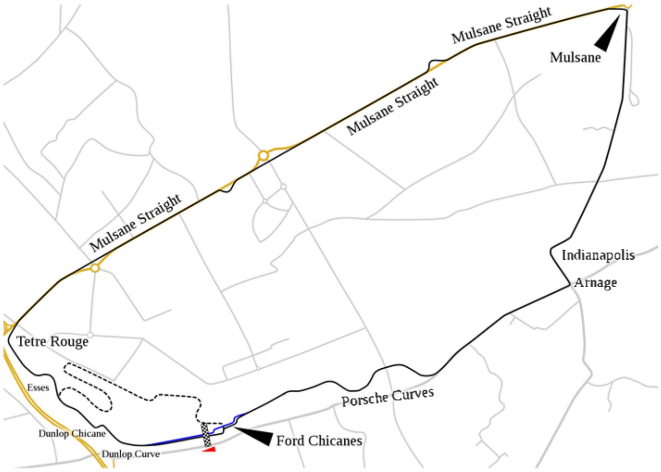

Fig. 2. Circuit de la Sarthe. Le Mans, France

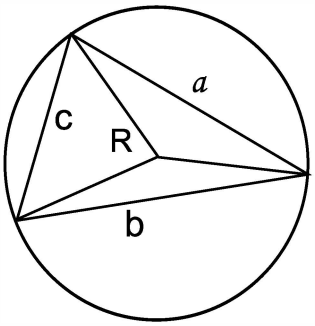

Fig. 3. Circumradius R of three points consitituting a triangle having lengths of a,b and c

A. Track layout

As mentioned in Section I, the track to be driven is the Circuit de la Sarthe, which is shown in Fig. 2. Using Google Earth [12] and 3D Route Builder [13] from Hybrid GeoTools, the raceline across the circuit was identified and a GPS map including the altitude at each point was extracted. This GPS map was then converted to a list of radii by calculating the circumradius of every three points as shown in Fig. 3 using [14]:

$$K = \sqrt{s(s-a)(s-b)(s-c)}, \tag{1}$$

where a, b, and c are the lengths (in m) of the sides of the triangle made of the three points and

$$s = \frac{1}{2}(a+b+c) \tag{2}$$

Finally, the radius R (in m) is calculated with:

$$R = \frac{abc}{4K} \tag{3}$$

The radius calculated is said to be the radius of the middle point (i.e., point between sides a and b). The left hand corners were defined to be positive and right hand to be negative. The track layout, with all its parameters is shown in Fig. 4. Once the track layout was defined, the next step was to identify the

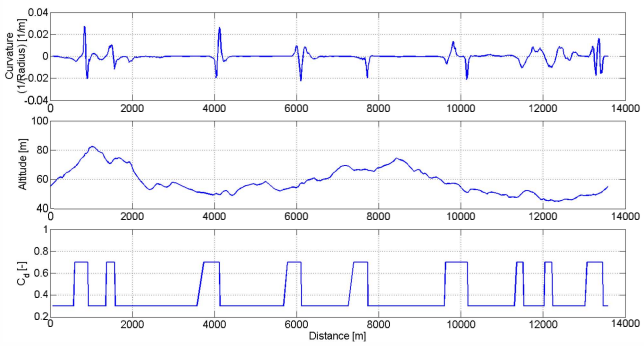

Fig. 4. From top to bottom: Inverse radius to clearly identify the corners; Altitude; Drag coefficient.

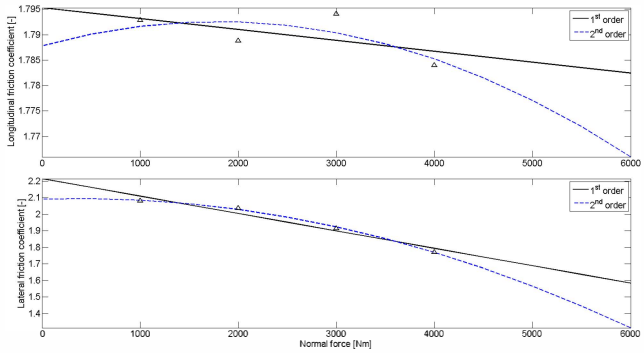

Fig. 5. 1st and 2nd order fit on Dunlop Formula 3 tire data.

tire friction coefficients, which determine the maximum speed achievable in the drivecycle.

B. Tire friction coefficients

Other necessary inputs are the longitudinal and lateral friction coefficients of the tires. Dunlop Formula 3 tire data was chosen for design; on which a linear and quadratic fits were created as shown in Fig. 5. The difference between the linear and quadratic fit was negligible up to a normal force of 4000 N (0.002 and 0.025 for the longitudinal and lateral friction coefficient respectively). Therefeore, the linear fit was chosen because of its simplicity. The friction coefficients in lateral and longitudinal directions are

$$\mu_x = 2.21 + (-1.05) \cdot 10^{-4} \cdot F_z, \tag{4}$$

$$\mu_y = 1.80 + (-2.14) \cdot 10^{-4} \cdot F_z, \tag{5}$$

where F_z represents the normal force acting on the tire (in N). Once the tire friction coefficients were defined, the limits on the lateral force that could be generated by the tires could be determined.

C. Lateral force limit of the tires

The cornering velocity of a race car is fully defined by the maximum lateral force the tires can handle before losing grip. Therefore, tire friction coefficients are used to determine the

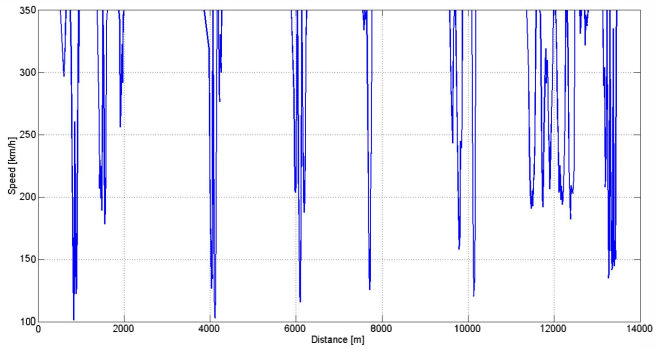

Fig. 6. Maximum velocity due to the lateral tire limit.

maximum velocity as a function of the radius. This is done by limiting the centrifugal force, F_y (in N), to the maximum allowable lateral force on the tires, $F_{y,max}$. The result of this step is shown in Fig. 6. Assuming steady state cornering, we can write

$$F_y = \frac{m \cdot v^2}{abs(R)}, \tag{6}$$

where m (in kg) is the mass of the race car and v (in m/s) is the velocity. Limiting F_y to the maximum lateral friction gives

$$F_{y,max} = F_{y,f} + F_{y,r} = F_y, \tag{7}$$

where $F_{y,f}$ and $F_{y,r}$ (in N) are the maximum front and rear lateral forces (distributed equally over the two front/rear tires), given by

$$F_{y,f} = \mu_{y,f}(F_{z,f}) \cdot F_{z,f}, \tag{8}$$

$$F_{y,r} = \mu_{y,r}(F_{z,r}) \cdot F_{z,r}. \tag{9}$$

Assuming a linear fit to the tire data, $\mu_{y,f}$ and $\mu_{y,r}$, the tires' lateral friction coefficients, can be expressed as

$$\mu_{y,f} = c_3 + \frac{c_4}{2} \cdot F_{z,f}, \tag{10}$$

$$\mu_{y,r} = c_3 + \frac{c_4}{2} \cdot F_{z,r}. \tag{11}$$

Here the coefficient c_4 is divided by two, to account for the fact that the tire data is for a single tire. For the normal forces $F_{z,f}$ and $F_{z,r}$ we can then write

$$F_{z,f} = \frac{(m \cdot g + F_{down}(v)) \cdot L_r}{L}, \tag{12}$$

$$F_{z,r} = \frac{(m \cdot g + F_{down}(v)) \cdot L_f}{L}, \tag{13}$$

where m is the mass of the race car (in kg), L is the length of the race car (in m), and L_f and L_r are the lengths from the center of gravity to the front and rear axle (in m), respectively. F_{down} is the downforce of the race car (in N) and is dependent on the speed according to

$$F_{down} = \frac{1}{2} C_{dd} \cdot \rho_{air} \cdot A_f \cdot c_d \cdot v^2, \tag{14}$$

with C_{dd} being the drag-to-downforce ratio, ρ_{air} the air density (in kg/m^3), A_f the frontal area of the race car (in

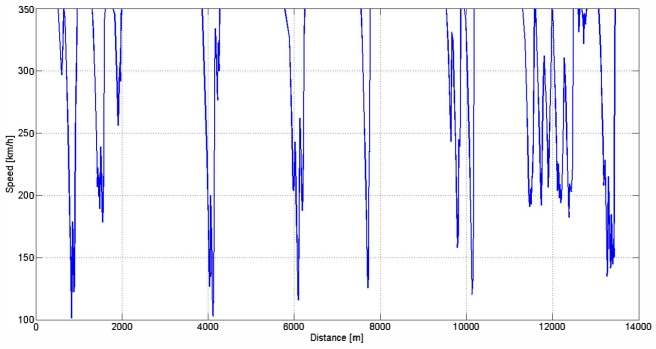

Fig. 7. Maximum velocity due to the lateral tire limit and brake limit.

m^2), and c_d the drag coefficient.
After considering the limits on speed imposed by the lateral force generated by the tires, the next step was to account for the limits imposed on the achievable speed by the available braking force.

D. Brake limit

Any race car has limited braking capabilities, which limits the allowable velocity at a time instant that precedes braking. Having the velocities given by lateral tire limits at each GPS position, the track is scrutinized in a backwards fashion. First, the final GPS position is analyzed, after which the previous GPS position is analyzed, and so on. At every point, it is checked whether the velocity is limited by the brakes or lateral force limit of the tires. This is represented by

$$v_{max} = min(v_{braking}, v_{lat}). \tag{15}$$

This limit then becomes the new maximum velocity and the new initial velocity for the next point. The result is shown in Fig. 7. The maximum deceleration, a_{min} (in m/s^2), is dependent on the longitudinal component of the gravitational force, F_g (in N), the friction force, F_f (in N), the drag force, F_d (in N), and the brake force, F_b (in N) as

$$a_{min} = -\frac{F_g + F_f + F_d + F_b}{m}. \tag{16}$$

Here, the longitudinal gravitational force as a function of the gradient θ (in rad) is given by

$$F_{g,x} = m \cdot g \cdot \sin(\theta), \tag{17}$$

the friction force is expressed as

$$F_f = c_d \cdot \cos(\theta) \cdot (m \cdot g + F_{down}), \tag{18}$$

the drag force can be written as

$$F_d = \frac{1}{2} \cdot \rho_{air} \cdot A_f \cdot c_d \cdot v^2, \tag{19}$$

and the brake force is written as

$$F_b = F_{x,f} + F_{x,r}, \tag{20}$$

where $F_{x,f}$ and $F_{x,r}$ are the front and rear longitudinal forces (in N) given by

$$F_{x,f} = \mu_{x,f}(F_{z,f}) \cdot F_{z,f} \tag{21}$$

$$F_{x,r} = \mu_{x,r}(F_{z,r}) \cdot F_{z,r}. \tag{22}$$

Assuming a linear fit to the tire data, $\mu_{x,f}$ and $\mu_{x,r}$, being the tires' longitudinal friction coefficients, can be expressed similar to equation (10) as

$$\mu_{x,f} = c_1 + \frac{c_2}{2} \cdot F_{z,f}, \tag{23}$$

$$\mu_{x,r} = c_1 + \frac{c_2}{2} \cdot F_{z,r}. \tag{24}$$

The normal forces $F_{z,f}$ and $F_{z,r}$ can be written as

$$F_{z,f} = F_{z,total} - F_{z,r} = F_{g,z} + F_{down} - F_{z,r}, \tag{25}$$

$$F_{z,r} = \frac{-B + \sqrt{B^2 - 4 \cdot A \cdot C}}{2 \cdot C}, \tag{26}$$

with:

$$\begin{aligned} A = &-F_{z,total} \cdot (L_f + c_1 \cdot h_{cog}) + \\ &2h_{cog}(F_{g,z}^2 + 2F_{g,z} \cdot F_{down} + F_{down}^2), \end{aligned} \tag{27}$$

$$B = L - 2 \cdot c_2 \cdot h_{cog} \cdot F_{z,total}, \tag{28}$$

$$C = 2 \cdot c_2 \cdot h_{cog}, \tag{29}$$

and the gravitational force in direction perpendicular to the surface, $F_{g,z}$ (in N) given by

$$F_{g,z} = mg \cdot \cos(\theta). \tag{30}$$

Once the limits imposed by the available braking force were taken into account, the next step was to consider the achievable acceleration.

E. Acceleration limit

The acceleration limit is mainly due to power and traction limitations and can be expressed as

$$\min((F_m - F_d - F_{g,x} - F_f), F_{x,max}), \tag{31}$$

where F_m is the force the motor can apply on the tires (in N), and $F_{x,max}$ is the maximum force the tires can handle (in N). F_m is written as

$$F_m = \frac{2 \cdot T \cdot M \cdot T_g}{D_{tire}}, \tag{32}$$

with T being the available torque at the current speed (in Nm), M the number of motors, T_g the gear ratio, and D_{tire} the tire diameter (in m). $F_{x,max}$ is written as

$$F_{x,max} = F_{x,f} + F_{x,r}. \tag{33}$$

See equations (21) to (30) for $F_{x,f}$ and $F_{x,r}$.

The drive cycle as calculated using the described method is shown in Fig. 8. As a comparison, the speed profile of the Le Mans Audi R18 e-tron quattro is added. Apparently, the largest time gain is at higher acceleration and higher top speed. The corner speed is usually very similar. This is most likely due to the high vehicle mass and Formula 3 tire data. The corners where the speed of the InMotion race car is much higher can be because of a low grip surface on the real race track or driver limitation. Also corner dynamics (i.e., load transfers) are not

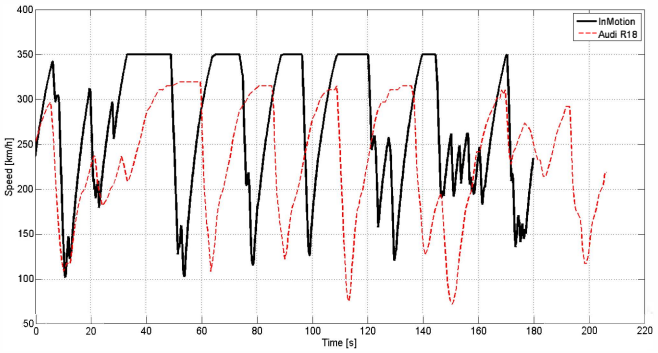

Fig. 8. Drive cycles on Circuit de la Sarthe for InMotion and the Audi R18 e-tron quattro.

taken into account, which would change the real cornering speed.

Once the process of deriving the drive cycle was set up, the next step in the design process was the selection of the technology of the powertrain components which is described in the following section.

IV. Selection of Technology

This section concerns the selection of technology for the InMotion series-hybrid racing car. The input for the selection were InMotion's goals from the powertrain, as described in Section I, the performance requirements and constraints, as described in Section II, and the drive cycle generated in Section III. IV-A describes different modes and the characteristics of the series hybrid topology. Once the hybrid powertrain topology is laid down, the technology choices for each powertrain component are described. IV-B presents the selection of the motor for the powertrain. IV-C presents the design of the fix ratio gearbox. IV-D shows the choice of the internal combustion engine. IV-E describes the considerations with regard to choosing the technology for energy storage, the reason for chosing ultracapacitors and the sizing of the ultracapacitors. In the last part in this section, IV-F, an electrical analysis of the powertrain is performed.

A. Topology

InMotion specified a series hybrid topology without plug-in capabilities for the race car. This topology is shown in Fig. 9. The reason for this specification is to create a research platform, which while being mechanically simple relative to other hybrid topologies, gives the possibility of testing new mobility-related technologies. The topology can be operated in different modes:

- ICE mode: All the power is delivered by the ICE.
- Hybrid mode: Both the ICE and the energy storage system provide power to the motors.
- Power split mode: The ICE supplies power to the motors and the energy storage system.
- Regenerative braking mode: The power generated while braking is stored in the energy storage system.

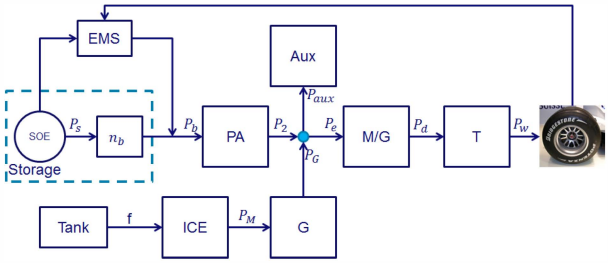

Fig. 9. Series topology, T = Transmission, M/G = Motor/Generator, Aux = Auxiliary power demand, G = Generator, ICE = Internal Combustion Engine, PA = DC/DC converter, EMS = Energy Management Strategy, SOE = State of Energy.

TABLE II. Motor parameters of the potential candidates. *Calculated with maximum continuous power. ** Calculated with maximum continuous torque.

Motor	UQM 200	EVO 240	Yasa 400	Yasa 750
Max Peak Power [kW]	200	335	165	100
Peak Torque [Nm]	900	1200	400	750
Max RPM	5500	5000	7500	2000
Rated RPM	1250	4000	3500	1250
Max Cont. Power [kW]	115	150	90	55
Max Cont. Torque [Nm]	450	440	245	420
Mass [kg]	95	80	20	25
Specific Power* [kW/kg]	1.2	1.4	4.5	2.2
Specific Torque** [Nm/kg]	4.7	5.5	12.3	16.8

B. Motors

There are a number of electric machine types that are suitable for traction applications, for example, induction machines, switched reluctance machines and permanent magnet synchronous machines. This paper focuses on permanent magnet synchronous machines due to their high efficiency and torque density [8], [15]. Four different motors were selected as potential candidates: UQM PowerPhase 200, Evo AFM-240, Yasa 400, and Yasa 750. The respective parameters of these motors can be found in Table II. It cannot be assumed that the motor with the highest specific power is the most suitable. First, it is required to take the gear mass into account. The gear mass is dependent on the gear ratio and maximum torque. Dependent on the maximum speed of each motor type and the required top speed, the gear ratio, and therefore the gear mass, varies. This will determine the specific power of the motor-gearbox combination, which is much more indicative. Second, the required power, and thus the total number of motors, is dependent on the mass and drag coefficient of the race car. Since the number of motors can only be an integer number, the total power might be too high at the cost of additional mass. Mass is a very important factor, therefore, this was considered a negative effect.

The requirement in Section II states that it is required to accelerate faster than a Formula 1 car. From this requirement, Section III-E shows that the required power is known for a specific mass and drag coefficient. With this knowledge, a feasibility analysis was performed. This analysis calculates the speed-torque operation points for the whole drive cycle (as presented in Section III) for each vehicle mass, M_v, and for each drag coefficient, C_d. For each M_v-C_d combination,

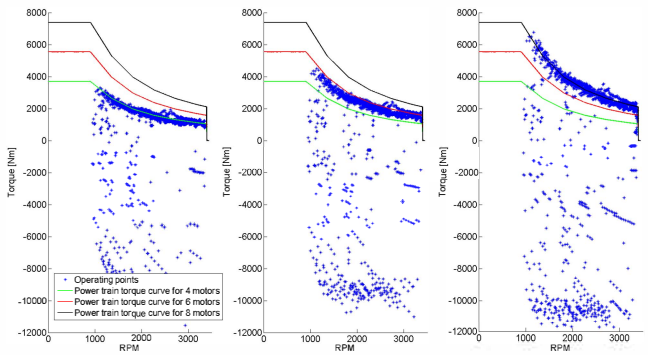

Fig. 10. Selection of required amount of motors to include all operating points, From left to right: $C_d = 0.3$, $M_v = 1300$ kg; $C_d = 0.5$, $M_v = 1400$ kg; $C_d = 0.6$, $M_v = 1800$ kg

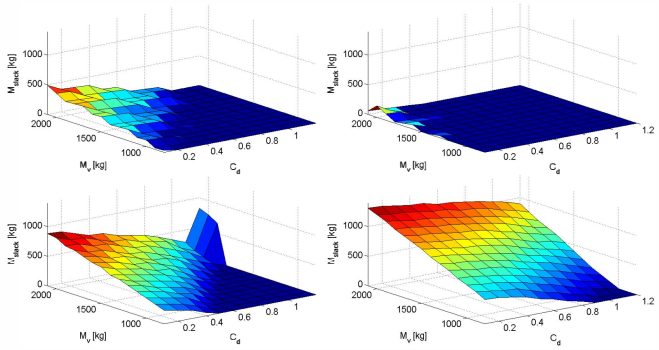

Fig. 11. Feasibility analysis' mass slack results, Top Left: UQM200; Top Right: EVO 240; Bottom Left: Yasa 750; Bottom Right: Yasa 400.

the number of motors required to cover all the operation points is calculated (see Fig. 10) as is the gear ratio. Together with a scaled ICE and generator, the total mass of the powertrain, M_{pt}, is obtained. If the mass of the powertrain is significantly lower than the corresponding mass of the race car, the configuration is assumed feasible. These calculations were performed using an assumed chassis mass of 400 kg. The results of this analysis are shown in Fig. 11. The excess mass (henceforth referred to as slack mass) is defined as $M_{slack} = M_v - M_{pt}$. For clarity purposes, all the negative slack masses are made zero.

As can be seen from Fig. 11, the Yasa 400 has the most slack and is therefore the most feasible. However, the number of Yasa 400's needed is not yet apparent. Looking at Fig. 10 again, it can be seen that in several situations, it is possible to reduce the number of motors by two compared to the initial feasibility analysis. The left figure, for example, shows the operating points of the drive cycle with a C_d of 0.3 and a M_v of 1300 kg. For the feasibility analysis all these operating points should be covered, resulting in a configuration with six motors. However, assuming that operation of the motors slightly above their continuous power is possible, it is just as feasible to use only four. A more detailed analysis on the different combinations is presented in Sections V and VI.

The generator was chosen to be the YASA 400 because of its high power to mass ratio, as shown in Table II.

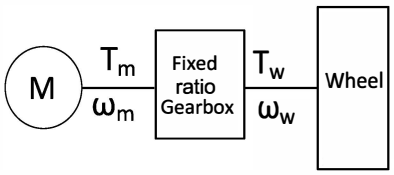

Fig. 12. Motor, Gearbox and wheel

Once the appropriate traction motors were selected, the transmission or reduction gear between the motor and the wheel was investigated.

C. Transmission

This section presents the calculation of the required mass of the transmission of the InMotion race car. To use the full maximum power range of the YASA 400, the transmission was designed to match the maximum speed of the motors to the maximum speed of the wheels. The purpose of this section is to find the mass for the transmission. Four fixed-ratio gearboxes connect each motor to its corresponding wheel as shown in Fig. 12. In the case where more than one motor are used for one wheel, the motors can still be connected to this wheel by one gearbox. Therefore four gearboxes will still be sufficient. The result shows that the mass is proportional to the torque at the wheels and does not depend on the number of motors.

There are two different considerations about gearboxes. First, is to choose either a spur gear or a helical gear. Second, is to choose between a simple gearbox with two gears or a planetary gear set. A spur gear type was chosen instead of a helical gear type because it is more durable and requires a smaller casing. Further, spur gears have less surface area when the gears are connected together compared to helical gears, and hence, create less friction. Although a helical gear is stronger than a spur gear because of a wider contact area, the helical gear produces a thrust load. This thrust load decreases the strength and durability of the gearbox.

The maximum rotational speed at the wheel is calculated as

$$\omega_{wheel} = \frac{v_{max}}{R_w} = \frac{100}{0.275} = 364(rad/s), \qquad (34)$$

where v_{max} is the maximum speed at the wheel, which equals to the top speed of 350 km/h with an additional safety margin of 10 km/h, R_w is the wheel radius. Thus the maximum speed of the wheel is 3472 rpm. The reduction ratio η_r was calculated to be 0.47 from the maximum speed of the Yasa 400 (7500 rpm) and from the maximum speed at the wheel. This ratio is achievable by a planetary gear if the input shaft connects to the sun gear and the output shaft connects to the planet carriers. Assuming that the planet gear has more than 10 teeth, this configuration requires a minimum of 160 teeth at the sun gear. This makes the gearbox rather big. Hence, the simple two gear spur gearbox was chosen.

To design the gearbox, the LEWIS formula [16] was used. The maximum load, W (in N), that does not cause teeth failure

for spur gear is given by:

$$W = \frac{S \cdot F \cdot Y \cdot g}{P} \frac{3.05}{3.05 + V}, \tag{35}$$

where S is the safe material stress ($28.1 \times 10^6 \frac{kg}{m^2}$ for steel 40C alloy [16]), F is the face width (in m), Y is the tooth form factor which depends on number of teeth, P is the pitch diametral (in m), and V is pitch line velocity (in m/s). The maximum torque is applied at a pitch line velocity between 0 and 1.53 m/s. To calculate the maximum load, it is therefore decided to use a velocity of 1.53 m/s. The pitch diametral is expressed as

$$P = \frac{N}{D}, \tag{36}$$

where N is the number of teeth and D is the gear diameter. The tooth load is expressed as

$$W = \frac{2T}{D}, \tag{37}$$

where T is the torque (in Nm), and D is the gear diameter (in m). Furthermore, it is assumed that each gear mass can be reduced by 50%, for example, either by making some holes or decreasing the width of the carrier, and that the mass of the housing is 40% of the mass of gear. The total gearbox mass, m (in kg), is calculated using

$$m = 1.4 * 0.5 \cdot \pi \cdot \rho \cdot \frac{F \cdot D^2}{4} \tag{38}$$

where ρ is the material density (in $\frac{kg}{m^3}$), and D is the gear diameter (in m).

By substituting 36 and 37 into 35, putting it in terms of D^2, and substituting that into 38, the total gearbox mass is expressed as

$$m = \frac{0.7\pi}{4} \frac{3\rho \cdot N \cdot T}{g \cdot S \cdot Y} \tag{39}$$

where N represents the number of teeth, T the torque at the gear (in Nm), and g the acceleration due to gravity (in $\frac{m}{s^2}$). This equation can be used to calculated the mass of the smaller and the bigger gears. The mass of the bigger gear is

$$m_1 = \frac{0.7\pi}{4} \frac{3\rho \cdot N_{max} \cdot T_w}{g \cdot S \cdot Y}, \tag{40}$$

where N_{max} is the number of teeth at this gear, T_w is the torque at the wheel. In a gearbox, the torque ratio between two gears equals to the teeth ratio between the associated gears. Because the reduction ratio is smaller than 1. The bigger gear is connected to the wheel. The mass of the smaller gear is

$$m_2 = \frac{0.7\pi}{4} \frac{3\rho \cdot r_g^2 \cdot N_{max} \cdot T_w}{g \cdot S \cdot Y}, \tag{41}$$

where r_g is the gear ratio. The total mass of the gearbox is

$$m_{total} = m_1 + m_2 = \frac{0.7\pi}{4} \frac{3\rho \cdot N_{max} \cdot T_w \cdot (1 + {r_g}^2)}{g \cdot S \cdot Y} \tag{42}$$

It can be seen in 42 that the required gear mass depend on the number of teeth at the bigger gear and the maximum torque at the wheel. If four YASA 400 motors are chosen, the maximum T_w is

$$T_{w,max} = \frac{4 \cdot T_m}{\eta_r} = \frac{4 \cdot 400}{0.47} = 3404Nm \tag{43}$$

As in [16], $\rho = 7850$kg/m^3 for Alloy steel, N_{max} is chosen as 30, Y = 0.3, $S = 28.1 \cdot 10^6\ kg/m^2$. Equation 42 leads to the total gear mass as 20 kg. Later, 42 is used for the lap time sensitivity analysis in Section V.

Another approach would be to integrate the transmission into the motor, as described in [9]. Which would diminish the mass of the total system and incorporate some degree of fault-tolerance.

D. ICE

Different ICEs were investigated in order to select a feasible engine for this study. The criteria for the chosen engine included: power to mass ratio, speed which gives maximum power, and engine durability. The speed is matched to that of the selected generator. There are two possible engines with high power to mass ratio and maximum power; they are the BMW V10 3L P84/5 [17] and the Audi 5.5L V12 TDI DPF [18]. The BMW P84/5 is designed for Formula 1 cars and has a power to mass ratio of 7.5 kW/kg. The Audi V12 TDI is designed for the Audi Le Mans race car and has 522 kW at 3000-5000 rpm and a mass of about 200 kg, giving it a power to mass ratio of 2.6 kW/kg. Although the BMW P84/5 has a higher power to mass ratio, the Audi 5.5L V12 was chosen because its durability. The speed of this engine matches with the speed of the YASA 400, which was chosen for the generators.

E. Energy storage

Energy storage is a crucial aspect of hybrid electric vehicles, since they aid the ICE as a secondary source of energy. This offers the possibility of reducing the fuel consumption of the engine and reducing the overall evergy loss in the powertrain be storing the energy recovered by regenerative braking. The role of energy storage in the architecture of the InMotion race car is to capture regenerative braking energy and apply it for acceleration. The energy storage has to be a lightweight, high power, and efficient source of electrical power. Moreover, the charge and discharge times should be as short as possible.

The energy storage technologies considered were batteries and ultracapacitors. Batteries posses a higher energy density than ultracapacitors, however, they are relatively limited in their power density. Furthermore, they have a relatively lower cycle life when compared to ultracapacitors. Hence ultracapacitors were chosen as the technology for energy storage. They satisfy the mentioned requirements and they can deliver frequent pulses of energy without any self-detrimental effects [19]. From the two types of ultracapacitors (symmetrical and asymmetrical), asymmetrical ultracapacitors (EDLC - Electrochemical Double Layer Capacitors) were chosen. This type of ultracapacitor stores the energy in the form of electrostatic charge by non-faradaic electric processes. Hence, it can be

TABLE III. Technical parameters of one pack (in a total two packs are needed)

Parameter	Value / Units
Number cells in series	99
Number cells in parallel	2
Voltage	267.3 V
Current	1368 A
Resistance	0.02327 Ω
Capacitance	30.3030 F
Weight (without frame)	55.44 kg
Max energy	0.3007 kWh
Volume (without frame)	0.062 m^2

charged very quickly and, unlike batteries, can be totally discharged without getting damaged [19].

Initial sizing of the ultracapacitors was done based on the voltage range of the DC-DC converter (200 - 530 V), the ultracapacitor cell characteristics, and the required charge and discharge power during acceleration and regeneration (i.e., braking). The regeneration power was obtained from the maximum power limit, as seen in Section VI. Based on the charge and discharge power requirements, the BCAP1500 ultracapacitor of Maxwell Technologies was chosen [20]. This type has a usable specific power of 6900 W/kg per cell, can sustain many cycles (100-1000 times), has a high efficiency during charge and re-charge, and has a high range of operating temperatures (-40°C to 65°C). The resulting arrangement of the energy storage are two packs of ultracapacitors which meet the maximum volume requirement mentioned in Section II. The corresponding data can be found in Table III.

For the energy management system, it is important to obtain an efficiency map of the suggested energy storage. Therefore, a simple RC circuit was modeled in order to simulate ultracapacitor pack behavior.

F. Preliminary electrical analysis of the powertrain

Once the technologies for the various powertrain components was selected, it was also essential to analyze the impact of the functioning of various electrical powertrain components on one another. Hence a preliminary electrical analysis of the powertrain was performed. For this analysis, a powertrain with eight motors, eight generators, four DC-DC converters, eight DC-AC converters, one energy storage system and four sets of DC-link capacitors was considered. Fig. 13 displays part of this electrical scheme, including the values of the voltages. The working voltage of the motors is 700 V, of the DC-DC converter 200-530 V. The upper limit on ultracapacitor operating voltage is determined by the state-of-charge, which should not be for safety reasons above 80%. The lower limit on voltage is determined by the value of DC-DC converter working voltage with a small safety margin. Thus the voltage operating range of the ultracapacitors is 213.8 and 427.6 V.

The energy flow in the system is bi-directional, thus motors operate in both motoring and generating mode. During the motoring mode, energy is supplied from the DC-link to the motors. If the energy request is higher than the energy that can be delivered, the voltage on the DC-link will drop significantly, limiting the power produced by the motors. During

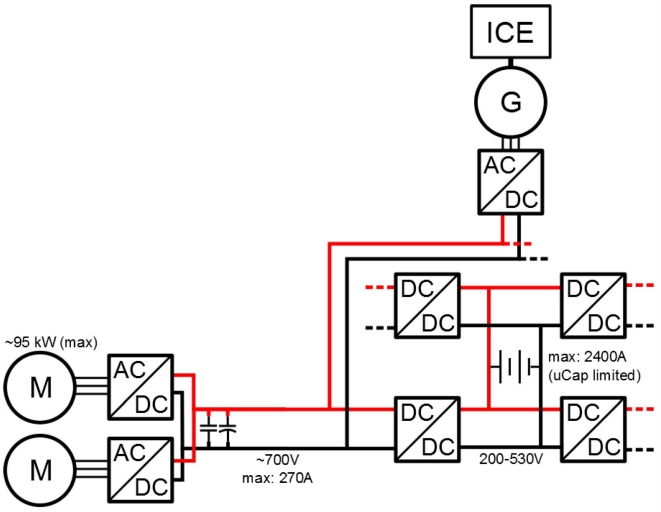

Fig. 13. Part of the electrical scheme of the powertrain architecture

the generating mode, the energy should be stored fast enough to avoid a rapid rise in voltage on the DC-link, which would damage the components.

The motors are capable of a more dynamic operation when compared the DC-DC converters and the ICE coupled with the generator. This difference in dynamics could cause the DC link to fail. To make sure that the DC-link can still handle these dynamics, sets of capacitors installed at close proximity to the motors has to be added. These sets should consist of both electrolytic and ceramic capacitors. The former is to add capacity; the latter is to handle the power.

To calculate the exact amount of DC-link capacitors needed, a full analysis of the dynamics of the system should be performed. This full analysis of the dynamics was not part of this research and is recommended for future research.

This section has introduced the selection of the topology, motors, transmission, internal combustion engine and ultracapacitors that satisfy the necessary requirements of InMotion. Once the technologies of the powertrain components were selected and a preliminary electrical analysis was performed, a preliminary investigation into the sizings of the various powertrain components was performed to minimize the laptime. This is described in the next Section.

V. Lap Time Sensitivity Analysis

A key requirement from the powertrain was to achieve a lap time of 2 min 45 s. Once the technologies for the powertrain were selected, the next logical step in the design was to size the powertrain components such that the lap time can be minimized. However there was no direct relation between the size of the powertrain components and the performance of the vehicle. This was because increased sizes of the powertrain components meant an increase in mass of the race car, thus sometimes reducing the performance. Aerodynamic characteristics also had a significant impact on the performance of the vehicle. Hence a sensitivity analysis was performed in order to gain insight into the impact of component sizings

TABLE IV. Masses of different components

Components	Masses
DC/DC converter	33 kg x 4
Ultracapacitors	200 kg
Chassis	400 kg
Motor	23 kg
Generator	23 kg
ICE	1 kg/2.6 kW

TABLE V. Number of generators, ICE power and mass, and total mass of the car for different number of motors

n_m	n_g	P_{ice} [kW]	m_{ice} [kg]	Car mass [kg]
4	5	548.1	211	1247
6	8	822.15	316	1473
8	10	1096.2	422	1677
10	12	1370.2	527	1880

and aerodynamic characteristics on the laptime of the vehicle. Three parameters were considered for the sensitivity analysis. The first parameter was the number of motors n_m, since this determined the sizes of the other powertrain components and hence the vehicle mass. The second and third parameters were the drag coefficient c_d and the the drag-to-downforce ratio C_{dd}, since these are the key aerodynamic characteristics of the race car. The number of motors n_m was varied as 4, 6, 8, or 10. The drag coefficient c_d was varied as 0.3, 0.4, 0.5, 0.6, or 0.7 and the drag-to-downforce ratio C_{dd} was varied as 3, 6, 9, or 12. A higher drag coefficient c_d will cause higher drag force and smaller acceleration. However, a high drag coefficient c_d and a high drag-to-downforce ratio C_{dd} result in a higher down force and this increases the maximum speed at the corner. Thus, in total, 4 x 5 x 4 = 80 sets (combinations) of parameters were obtained. The mass of the powertrain components is presented in Table IV, where the mass of the gearbox is calculated from the maximum torque (39).

An average efficiency of 85% for motor and generator is incorporated in the drive cycle. This helps in accounting for the fact that more generators would be needed than motors, so as to compensate for losses. At the same time, this also helped in sizing the engine to approximately account for generator and motor losses. In addition, the engine is assumed to run at ϑ_{ice} = 90% of the maximum power. The reason is to have a safety margin when doing the matching with the backwards model, Section VI. Required number of generators and the ICE power are calculated with these equations:

$$n_g = \frac{n_m}{\eta_m} \tag{44}$$

$$P_{ice} = \frac{P_m \cdot n_m}{\vartheta_{ice} \cdot \eta_m^2} \tag{45}$$

where n_m is number of motors and η_m is motor efficiency. Table V presents the number of generators, total mass of the car and ICE power and mass for different number of motors.

The drive cycle presented in Section III determines the lap time for 80 different sets of parameters shown in Fig. 14. Each subplot shows the result for one drag-to-downforce ratio. It can be seen that the lap time decreases with increasing C_{dd}. When the value of drag-to-downforce ratio C_{dd} is 3, more motors results in decrease of lap time. However for higher values of C_{dd}, there are no significant differences between lap time for 8 motors and for 10 motors. For 4 motors, the lap time increases when c_d increases, that means the drag force at straights has more impact than the down force at the corners. For 6 motors, the lap time is the lowest when c_d = 0.5. For 8 and 10 motors, the lap time tends to decrease when c_d increases. It was found that using 8 motors with a drag-to-downforce ratio of 12 and a drag coefficient of 0.6, yielded the lowest possible lap time. However, using 8 motors, would require 10 generators and a relatively large engine, which would result in a heavy powertrain and a higher fuel consumption. Although InMotion had not specified any constraints on fuel consumption, the authors decided to include multiple sets of powertrain sizings, in order to clearly demonstrate the penalty on race car mass and fuel consumption as the lap time was decreased. Finally, four feasible sets of parameters were chosen and are shown in Table VI. The sets were selected because they yielded the lowest lap times among all possible combinations of parameters. Three sets have drag ratio C_{dd} of 9 and one set has C_{dd} of 12.

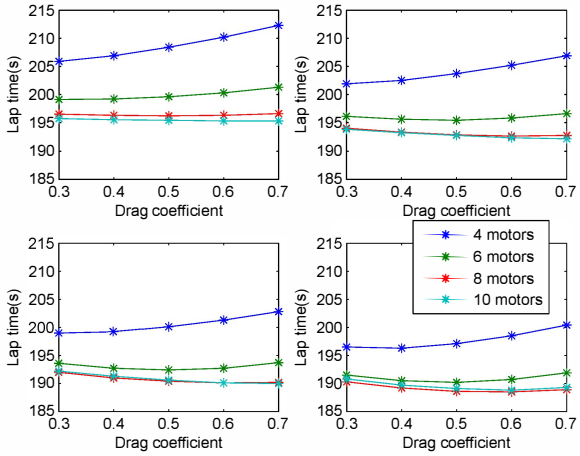

Fig. 14. From left to right and top to down: Lap time for drag-to-downforce ratio of 3, 6, 9, 12

To decrease the lap time, active aerodynamics was modeled by increasing the drag coefficient at the straights and decreasing it at the corners. This enhances both the acceleration limit and the limit on the lateral force that can be generated by the tire. A new analysis with active aerodynamics was done for four chosen sets, in which drag coefficient c_d is 0.7 at the corners and 0.3 at the straights. Table VI presents these four sets and the lap times with fixed and varied c_d. It can be seen that in all cases, active aerodynamics results in a reduction in lap time. Additional insight can be obtained by analyzing the acceleration profiles, as shown in Fig. 15. It can be concluded that only the car with 10 motors has a comparable profile to the Formula 1 car. Simulations showed that the cars with 4, 6, and 8 motors can have a Formula 1 - comparable acceleration

TABLE VI. Four sets of parameters. * c_d is 0.3 at straights and 0.7 at corners.

Set No.	n_m	C_{dd}	Lap Time (Constant c_d)	Lap Time (Active c_d *)
1	4	9	199.0 — 0.3	193.2 — 0.3-0.7
2	6	9	192.4 — 0.5	189.2 — 0.3-0.7
3	8	9	190.1 — 0.6	188.5 — 0.3-0.7
4	8	12	188.5 — 0.6	186.7 — 0.3-0.7

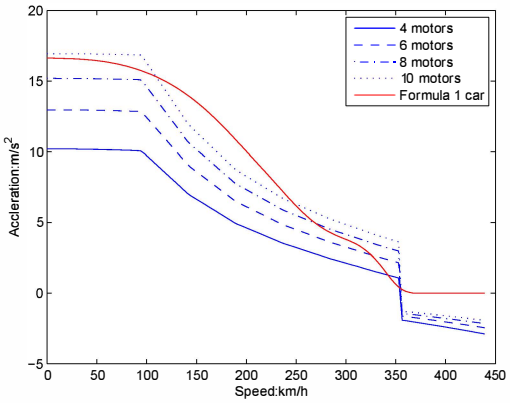

Fig. 15. Acceleration profiles of the cars with 4, 6, 8, 10 motors and the formula 1 car

profile if the mass of the car can be reduced 600, 400, and 200 kg respectively. It can be seen from Table VI that the lowest lap time (188.5 s), with the available technologies, is still 23.5 s above the requirement of being faster than 2 min 45 s (165 s). The acceleration profile of the model is worse than the acceleration profile of the Formula 1 car (2004 season). To decrease the lap time, the components masses should be reduced. Furthermore, the lap time may be reduced by the tires with higher friction capability than that of the Formula 3 tires used in the model.

Once the feasible powertrain component sizes have been defined, the next step is the design of an Energy Management System (EMS) which would optimize the flow of power between the powertrain components and help the race car achieve a high efficiency. In order to implement this EMS, the race car had to modeled. The modeling of the race car, as well as the design and implementation of the EMS on the feasible sets of powertrain sizes are described in the next Section.

VI. Modeling and Optimization

There are two major approaches to modeling vehicles: the forwards modeling approach and the backwards modeling approach. In the forward modeling approach, the vehicle model incorporates the physical characteristics of the various powertrain components. This approach accounts for the physical causality of the powertrain components, but increases the required computation time. The powertrain of the InMotion race vehicle was modeled using the backwards modeling approach. The main advantages of using this approach are

- Suitability for the design of supervisory control systems that optimize the power flow in the propulsion system.
- Reduction of computation time.
- Simplification of modeling of efficiency conversion between powertrain components.
- Reasonable accuracy of fuel consumption calculations [21].

The main drawback of using the backwards modeling approach is that the physical causality is not respected and therefore, dynamic effects are not properly addressed. However, this does not significantly impact the accuracy of the fuel consumption calculations [21]. The input variables come from the driving cycle calculation, which is explained in Section III. The force F_t acting on the wheels was computed taking into account the speed and acceleration required to drive the predefined drive cycle. After that, the power flow was estimated for the different powertrain components and finally, the fuel consumption to drive the predefined drive cycle was predicted. More information about the backwards modeling approach can be found in [21].

The powertrain was modeled using the backwards approach with the following assumptions:

- The driving cycle (speed profile) is known in advance.
- The vehicle runs at a constant speed and acceleration for a short period of time i, which was considered to be 0.1 s.
- The fuel tank mass is constant during the simulation.
- The transient response of the powertrain components is not included.

In this study, the backwards modeling approach was used to optimize the energy flow of the powertrain using different supervisory control strategies. Moreover, the backwards model helped in finding the trade-off between sizing the components, fuel consumption, and the impact on lap time. This is addressed in Section VI-C.

A. Modeling description

Based on the powertrain layout shown in Fig. 9, powertrain component input and output requirements were modeled using the backwards modeling approach. Vehicle dynamics were implemented using Newton's second law. The total force acting on the vehicle was calculated based on following equations:

$$F_{t,i} = m \cdot a_i + F_{r,i} + F_{a,i} + F_{g,i}, \tag{46}$$

where

$$F_{r,i} = m \cdot g \cdot \cos(\alpha_i), \tag{47}$$

$$F_{a,i} = \frac{1}{2} \cdot c_d \cdot \rho_a \cdot A_f \cdot c_d \cdot v^2, \tag{48}$$

$$F_{g,i} = m \cdot g \cdot \sin(\alpha_i), \tag{49}$$

where $F_{t,i}$ (in N) represents the force acting on the wheels, $F_{r,i}$ (in N) represents the rolling friction, $F_{a,i}$ (in N) the aerodynamic friction, $F_{g,i}$ (in N) the force caused by gravity when the road has an inclination angle α_i (in rad), A_f (in m^2) the frontal area of the vehicle, and ρ_a (in kg/m^3) the density of air. c_d is the drag coefficient, m is the vehicle mass, g is the acceleration due to gravity (in m/s^2) and a_i is the acceleration of the vehicle (in m/s^2).

The power at the wheels required to drive the predefined profile, $P_{w,i}$ (in W), was computed as follows:

$$P_{w,i} = T_{w,i} \cdot \omega_{w,i}, \tag{50}$$

where

$$T_{w,i} = F_{t,i} \cdot R_w, \tag{51}$$

$$\omega_{w,i} = \frac{v}{R_w}, \tag{52}$$

where $T_{w,i}$ represents the torque acting on the wheels (in Nm), $\omega_{w,i}$ the angular speed of the wheels (in rad/s), v the vehicle speed (in m/s) and R_w the wheel radius (in m). The power at the wheels is calculated by using the balance of forces acting on a vehicle in motion, see (46).

The power at the input of the gearbox $P_{d,i}$ (in W) was modeled with the following equation:

$$P_{d,i} = T_{d,i} \cdot \omega_{gb,i}, \tag{53}$$

with:

$$T_{d,i} = \begin{cases} \frac{T_{w,i}}{\eta_{gb}} \cdot r_g & T_{w,i} \geq 0 \\ T_{w,i} \cdot \eta_{gb} \cdot r_g & T_{w,i} < 0 \end{cases} \tag{54}$$

and

$$\omega_{gb,i} = \frac{\omega_{w,i}}{r_g}, \tag{55}$$

where r_g represents the gear ratio. The efficiency of the gearbox η_{gb} was assumed to be constant with a value of 0.98. The selection of the fixed gear ratio was done to match the maximum electric motor rotational speed with the maximum wheel speed due to the driving cycle. The value was calculated as $r_g = 0.47$.

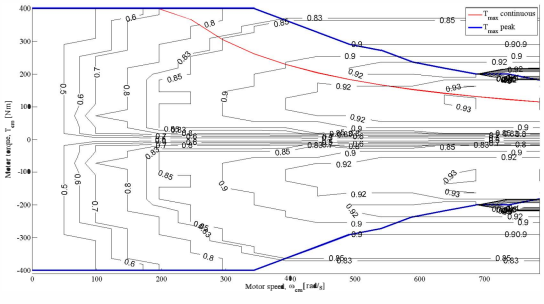

Fig. 16. Yasa 400 motor/controller efficiency map

The electric motor Yasa 400 was modeled by interpolation of the efficiency map shown in Fig. 16. The maximum power limit that can be obtained by regeneration was calculated using the power characteristic of the electric motor in the generating mode. The generator in the powertrain was modeled using the same efficiency map as the electric motor (Yasa 400), with the assumption that efficiencies in the generating regime are a mirror image of that in the motoring regime.

The energy storage device (ultracapacitors) was modeled using the efficiency map that was obtained from an RC model as described in Section IV-E, using the following equation:

$$P_{2,i} = \begin{cases} P_{b,i} \cdot \eta_{DC} & P_{b,i} \geq 0 \\ P_{b,i} / \eta_{DC} & P_{b,i} < 0 \end{cases} \tag{56}$$

where $P_{2,i}$ represents the output power of the DC/DC converters (in W) and $P_{b,i}$ the output power of the storage device (in W). The detailed description of the ultracapacitor design is explained in Section IV-E. The DC/DC converters were modeled with a constant efficiency of 0.97 [22].

The ICE was modeled using a scaled efficiency map of a 1.9 L TDI standard diesel engine [23] shown in Fig. 17. This was carried out to approximate the performance of the engine proposed in Section IV-D. The engine map for the proposed engine could not used because the data was not available. The ICE and the generator were combined in one efficiency map (genset) in the E-line tracking strategy, which is described in Section VI-B. The power flow between power sources and loads is shown in Fig. 9, where their electrical connection can be written using the following equation:

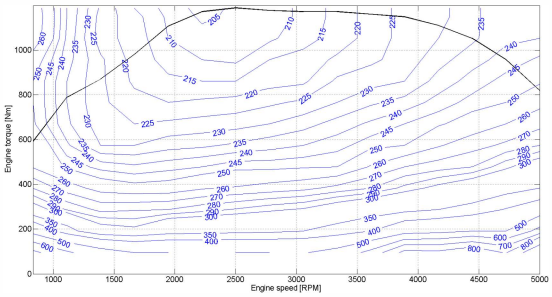

Fig. 17. Engine map [g/kWh]

$$P_{e,i} + P_{aux} = P_{2,i} + P_{G,i}. \tag{57}$$

The power for the electrical auxiliaries, P_{aux}, was assumed to be constant along the drive cycle, with a value of 40 kW.

The backwards vehicle model was used to design the energy management strategy that optimizes energy flow along the drive cycle, which is described in the next section.

B. Energy Managment Strategy (EMS)

Two energy management strategies were designed for the InMotion powertrain. One of the strategies is heuristic (Boost strategy) and the other is based on optimal control theory (Equivalent Consumption Minimization Strategy). The problem formulation and the descriptions of both methods are introduced in the following subsections.

1) Problem formulation: Energy management strategy was formulated as a numerical optimization problem, based on the discretized model of the vehicle presented at the beginning of Section VI (backwards model). It was solved by finding the optimal control law $u(k)^*$ that minimizes the cost function J which describes the total fuel consumption over the generated drive cycle with length N as described by:

$$u(k)^* = arg\ min\ J, \tag{58}$$

where

$$J = \sum_{k=0}^{N-1} L[x(k), u(k)]\Delta t = \sum_{k=0}^{N-1} [\dot{m}_f(k)]\Delta t; \tag{59}$$

subject to the following constraints:

$$x(k+1) = f(x(k), u(k)), \tag{60}$$

$$P_{ICE,i} \leq (T_{ICE,max} \cdot \omega_{ICE,max}), \tag{61}$$

$$P_{e,i} \leq (T_{M,max} \cdot \omega_{M,max}), \tag{62}$$

$$P_{s,min} \leq P_{s,i} \leq P_{s,max}, \tag{63}$$

$$SoE_{min} \leq SoE_i \leq SoE_{max}, \tag{64}$$

where SoE represents the storage device State of Energy with a minimum limit of $SoE_{min} = 0.4$ and a maximum limit of $SoE_{max} = 0.8$. These values were chosen as per the static electrical analysis of the powertrain, as discussed in Section IV-F. The instantaneous fuel mass flow used by the vehicle is represented by $L = \dot{m}_f(k)$. The state variable of the model is represented by $x(k)$, which is the SoE. The control variable is represented by $u(k)$, which is the input power of the storage device P_s (ultracapacitors), where

$$u(k) = P_s(k), \tag{65}$$

$$x(k) = SoE(k) = \sum_{k=1}^{N} \frac{P_s(k)}{E_0}, \tag{66}$$

where E_0 is the energy in the storage device at the beginning of the drivecycle.

In addition to the constraints mentioned above, the strategy should ensure a charge sustaining vehicle, where the energy level of the storage device at the end of the cycle ($t = t_e$) is equal to the one at the beginning ($t = 0$):

$$E_s(t_e) = E_s(0). \tag{67}$$

For the optimization, the genset was set to run on the E-line, which represents the operating points with maximum efficiency for every power demand, P_e, required from the wheels. This can be expressed as

$$P_{m,e-line} = \arg \min_{(\mathrm{T_m},\omega)\in\varrho(\mathrm{P_m})} f^{\circ}(T_m, \omega), \tag{68}$$

$$\varrho(P_m) = (T_m, \omega) | (P_m = T_m \cdot \omega), \tag{69}$$

where T_m and ω represent the operating points (torque and angular speed) of the ICE according to the E-line strategy (in Nm and rad/s respectively). The E-line strategy is ideal for the series hybrid configuration, since no mechanical connection exists between the engine and the drive line. This allows the engine to operate in the region where efficiency is maximum for a certain power request [24].

2) Boost strategy: This heuristic strategy was designed with the hypothesis that fuel can be saved by assisting the engine on the track regions where it needs to accelerate the vehicle right after the braking regions. In this mode, the ultracapacitors store as much energy as possible during the regeneration period. They deliver the stored energy directly afterwards, when traction power is required, until they completely discharge the stored energy. The advantage of using this strategy is the simplicity of control algorithm, which keeps the implementation efforts relatively low.

For this strategy, the control variable $u(k) = P_s$ is controlled as follows:

$$P_s(k) = P_{s,regen}(P_e(k)) \text{ if } P_e(k) < 0 \wedge SoE(k) < SoE_{max}, \tag{70}$$

$$P_s(k) = P_{s,MO}(P_e(k)) \text{ if } P_e(k) \geq 0 \wedge SoE(k) > SoE_{min}, \tag{71}$$

where $P_{s,regen}$ represents the input power of the storage device during the regeneration mode (in W) and $P_{s,MO}$ the input power of the storage device in full electric mode. Furthermore, this strategy is similar to the Kinetic Energy Recovery System (KERS) used currently in Formula 1 vehicles [1], with the difference that the energy is delivered completely after the regenerative braking mode.

3) Equivalent Consumption Minimization Strategies (ECMS): ECMS have been introduced in literature [25]. This optimization method is based on an equivalent fuel-mass flow $\dot{m}_{f,eq}(k)$ (in g/s). The equivalent fuel mass flow uses an equivalent weight factor $\lambda(k)$ (in g/J), which represents the mass of fuel needed for electric propulsion, or electric-energy-to-fuel-conversion-weighting-factor. The equivalent mass flow is expressed as

$$\dot{m}_{f,eq}(k) = \dot{m}_f(P_s(k), k) - \lambda(k) \cdot P_s(k) \quad \forall\ \lambda(k) > 0, \tag{72}$$

where $\dot{m}_f(k)$ is the actual fuel mass flow, which can be expressed as a function of the battery input power P_s.

Using this principle, the ECMS for the optimization problem was formulated as follows:

$$P_s^*(k) = \arg \min_{\mathrm{P_{s(k)}}} [\dot{m}_{f,eq}(k) \mid \lambda(k)], \tag{73}$$

where $\lambda(k)$ was optimally selected to satisfy the constraints presented in (72). The ECMS algorithm is based on optimal control theory using the Hamiltonian and/or Lagrangian multipliers [25]. ECMS is based on the principle that the sum of the current and future fuel savings should be higher than the future and current fuel cost [21].

C. Final component sizing

As mentioned in Section VI, one of the aspects for optimizing the powertrain is sizing. In this case sizing the powertrain refers to determining the power/energy rating and the number of components that are needed to ensure the delivery of the power required at the wheels. The sizing done at this stage

gives more accurate results that that done in Section V, since in this Section, the actual efficiencies of the components are taken into account in the model. The only scaled component is the engine.

The design of the engine was in the development phase by InMotion at the time of writing of this paper, and therefore, it was outside the scope of this research. This study aimed at providing the performance requirements and size of the engine model, which is presented in Section VI-A based on the technology mentioned in Section IV-D.

The size of the ultracapacitor stack was fixed to meet the performance required by regenerative braking, taking into account the restriction of maximum volume imposed by InMotion (see Section IV-E). Although the ultracapacitors could be downsized, this study assumes a fixed maximum volume mainly because of the maximum regeneration required and the restriction of the DC/DC converter voltage range. See Section IV-F.

For selecting the number of motors and generators, the parameters of the sensitivity analysis and the backwards model were synchronized. This was done to define the different possible combinations of motors/generators and aerodynamic parameters, as mentioned in Section V. The backwards model was used to validate the results of the sensitivity analysis by comparing the vehicle mass and looking at the operating region of the motors and generators given the corresponding driving cycle. Fig. 18 illustrates the process of selecting the possible solutions for the powertrain.

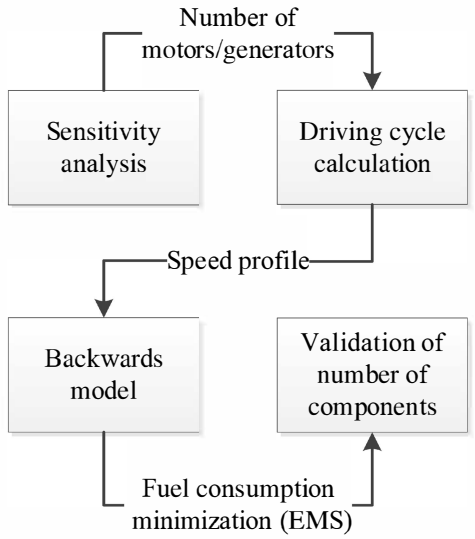

Fig. 18. Final component sizing process

D. Results

Four different sets of parameters were found in the sensitivity analysis, as mentioned in Section V. Table VII summarizes the results of the backwards model for each of the combinations. It can be seen that there is a trade-off between fuel consumption and lap time. In adddition, having more motors decreases the lap time at the cost of increasing the size and maximum power required of the ICE, which increases the fuel consumption. Moreover, it can be seen that varying c_d reduces the fuel consumption and lap time, compared to the fixed one. It is worth mentioning that, for simplicity, only one set with varying c_d was simulated with the backwards model (Set No. 3).

TABLE VII. Backwards model results for the four sets chosen. * Set No. 3_a refers to the simulation using constant c_d and 3_b using varying c_d

Set No.	Total mass [kg]	P_{ICE} max [kW]	ICE mass [kg]	FC ECMS [kg/lap]	FC Boost [kg/lap]	lap-time [s]
1	1242	537	206	3.71	3.95	199.0
2	1457	780	300	5.04	5.28	192.4
3_a*	1647	1021	393	6.17	6.38	190.1
3_b*	1652	1036	398	5.49	5.65	188.7
4	1634	988	380	6.05	6.29	188.5

For simplicity, only the results for solution 2 (6 motors, 8 generators, C_{dd}=9, c_d=0.6) are presented in this paper. Fig. 19 and 20 show the operating points for the motor and engine respectively.

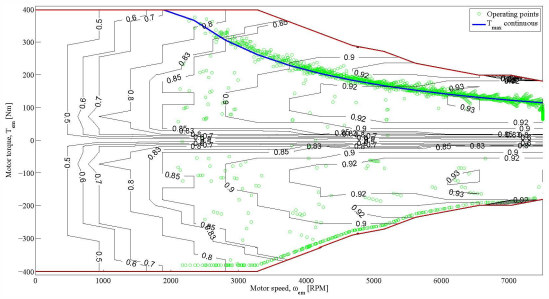

Fig. 19. Motor operating points

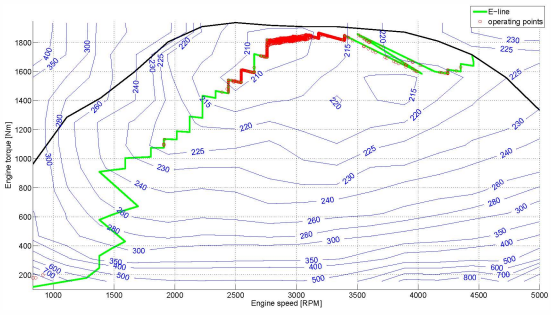

Fig. 20. Engine operating points

The control variable u=P_s (ultracapacitors input power) and the State of Energy (SoE) using the ECMS are shown in Fig. 21.

Fig. 22 shows the electric power required at the wheels P_e and the input power of the ultracapacitors P_s using the ECMS. Fig. 23 shows the same result for the Boost strategy.

To investigate the trade-off between fuel consumption and lap time, the number of theoretical laps that the InMotion vehicle would be able to complete was computed for every of

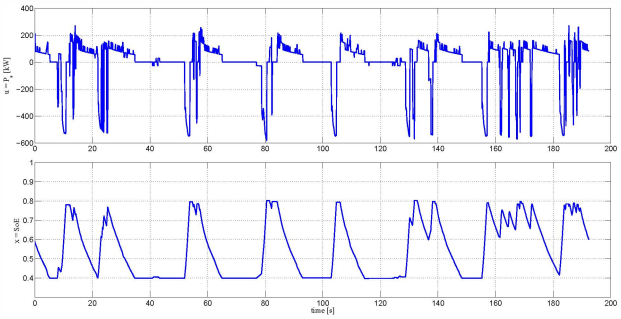

Fig. 21. Ultracapacitors input power using the ECMS

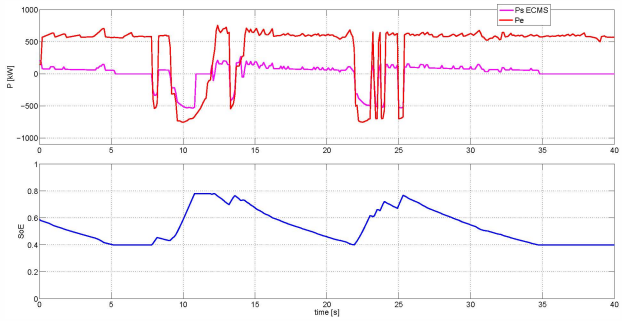

Fig. 22. From top to bottom P_s and P_e using the ECMS, SoE

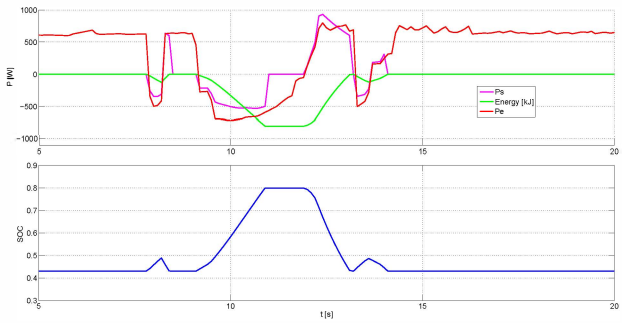

Fig. 23. From top to bottom P_s and P_e using the Boost strategy, SoE

the four sets presented in Table VII. Assuming a fuel density value of 0.83 kg/l [26] and a fuel mass of 75 kg per tank, the number of laps that the vehicle could complete was obtained. The total time per pit stop cycle was estimated by firstly, computing the number of times the vehicle needs to stop for refueling, and secondly, by adding the pit stop time, which in this case was assumed to be 60 s. Table VIII presents the results for the completed total number of laps for each of the fours sets for the powertrain, including the one where c_d is varied. It can be seen that there is an improvement of four laps (from 442 to 446 in Set No. 3) when c_d is varied. The number of laps that a Formula 1 car (2004 season) would be able to complete is also shown in Table VIII, based on a theoretical lap time of 175 s (see Section II) and a fuel consumption of 75 l/100 km [27].

It can be concluded from the results presented above that several options are feasible for designing the powertrain of

TABLE VIII. Theoretical results for the InMotion vehicle in Le Mans. *Set No. 3_a refers to the simulation using constant C_d and 3_b using varying C_d . **Based on FC=7.92 kg/lap.

Set No.	laps per tank	total no. of laps	no. of pitstops	total distance [km]
1	20	428	21	5833.2
2	15	440	29	5996.8
3_a*	12	443	37	6037.6
3_b*	14	447	32	6092.2
4	12	446	37	6078.5
Formula 1**	9	476	53	6487.4

the InMotion vehicle. The trade-off between fuel consumption and lap time can be better addressed once parameters of more appropriate tires are included in the model, and once more accurate efficiency data for the ICE map is obtained. Moreover, active aerodynamics (varying c_d) and increasing the drag-to-downforce ratio have a positive impact in reducing fuel consumption and lap time, as presented in Table VII and Table VIII.

VII. Conclusion

This paper presents an initial design of the powertrain for the InMotion IM01 race car. Several powertrain configurations were proposed, where several parameters were varied to investigate their impact on the lap time. A bicycle model was created and used to calculate a drive cycle. Different technology options for the powertrain components were researched and the most feasible options were chosen for the design. In addition, a backwards model was developed, including several efficiency maps, to calculate the overall fuel consumption over the predefined speed profile.

One part of InMotion's vision is to be 10 s faster than a Formula 1 car on Circuit de la Sarthe (i.e. 2 min 45 s, based on the 2008 season). However, with the model created, the fastest lap with one of the proposed configurations (Set No.4, see Table VII) was 3 min 9 s. The large mass was a key factor that prevented the race car with the designed powertrain from achieving the required lap time. In addition, it was found that using more than 10 motors would not reduce lap time. However, it is the belief of the authors that using parameters of more appropriate tires in the model will reduce the lap time. Further, using custom-built powertrain components, especially the traction machine, would significantly reduce weight and also contribute to reducing lap time.

Two energy management strategies were developed, Boost and ECMS, where the ECMS presented the optimum solution with a minimum fuel consumption of 3.71 kg/lap compared to 3.95 kg/lap for the Boost strategy (set No. 1, see Table VII). The percentage of fuel savings using ECMS when compared to Boost is between 2.8% and 3.7%. Further, the results show that having more motors reduces this relative fuel saving.

All the models and algorithms were made such that they are easily adaptable to any new insights.

The following recommendations are proposed:

- To ensure safe and reliable operation of the electrical components, a full electrical analysis of the powertrain

should be performed, as discussed in Section IV-F.

- To further reduce lap time and improve fuel economy, active aerodynamics should be applied.
- To allow higher cornering speeds and higher acceleration/deceleration in the simulation, more suitable tire models should be used.
- To reduce the overall vehicle mass, different possibilitites for components integration and reduction of chassis mass should be investigated.
- To enhance the quality of the model, more accurate efficiency maps for the generator, gearbox and ICE should be used.
- To ensure that the engine power level remains feasible and to reduce the total mass of the vehicle (see Table VII), a powertrain configuration with 4 motors should be used.

ACKNOWLEDGMENT

The authors would like to thank all members of the Electromechanics and Power Electronics group at the Eindhoven University of Technology (www.tue.nl/epe) for their feedback and support. Furthermore the authors would like to thank the InMotion team for their input and remarks and the ASD affiliates for their support.

REFERENCES

[1] Formula 1: *Kinetic Energy Recovery Systems (KERS)*, [Online]. Available: http://www.formula1.com/inside_f1/understanding_the_sport/8763.html; visited, 09.2012.

[2] Audi: *Audi R18 e-tron quattro*, [Online]. Available: http://www.audi.co.uk/audi-innovation/audi-motorsport/audi-r18-etron-quattro.html; visited, 09.2012.

[3] S. Lambert, S. Maggs, P. Faithfull, A. Vinsome, *Development of a Hybrid Electric Racing Car*, in Hybrid and Eco-Friendly Vehicle Conference, 2008.

[4] F.L. Mapelli, D. Tarsitano, *Energy control for Plug-In HEV with Ultracapacitors Lithium-Ion batteries storage system for FIA Alternative Energy Cup Race*, IEEE Vehicle Power and Propulsion Conference (VPPC), 2010.

[5] J. Sibley, A. Emadi, *A control analysis of high-performance hybrid electric vehicles*, IEEE Vehicle Power and Propulsion Conference (VPPC), 2010.

[6] K.W. Benson, D.A. Fraser, S.L. Hatridge, C.A. Monaco, R.J. Ring, C.R. Sullivan, P.C. Taber, *The Hybridization of a Formula Race Car*, in IEEE Conference Vehicle Power and Propulsion, 2005.

[7] J.J.H. Paulides, B.L.J. Gysen, K.J. Meessen, Y. Tang, E. Lomonova, *Influence of multiple air gaps on the performance of electrical machines with (semi) Halbach magnetization*, IEEE Transactions on Magnetics, 47(10), 2664-2667.

[8] E.A. Lomonova, E.V. Kazmin, Y. Tang, J.J.H. Paulides, *In-wheel PM motor: compromise between high power density and extended speed capability*, COMPEL: The International Journal for Computation and Mathematics in Electrical and Electronic Engineering, Vol. 30(2011), No. 1, p. 98-116

[9] T. Gerrits, C.G.E. Wijnands, J.J.H. Paulides, J.L. Duarte, *Fault-tolerant operation of a fully electric gearbox equivalent*, IEEE Transactions on Industry Applications, Vol. 48(2012), No. 6, p. 1855-1865

[10] F1 Fanatic: *How quick would F1 lap at Le Mans* [Online]. Available: http://www.f1fanatic.co.uk/2008/06/14/how-quick-would-f1-lap-at-le-mans; visited 01.2013

[11] YouTube: *One lap of the Circuit De La Sarthe with Marcel Fssler in the Audi R18 e-tron Quattro*, [Online]. Available: http://www.youtube.com/watch?v=DRJHYc3ubxI; visited, 09.2012.

[12] Google: *Google Earth*, [Online]. Available: http://www.google.com/earth/index.html; visited, 10.2012.

[13] Hybrid GeoTools: *3D Route Builder for Google Earth*, [Online]. Available: http://www.hybridgeotools.com/html/3d_route_builder.html; visited, 10.2012.

[14] Wolfram Mathworld: *SSS Theorem*, [Online]. Available: http://mathworld.wolfram.com/SSSTheorem.html; visited, 09.2012.

[15] Z. Q. Zhu and David Howe, *Electrical Machines and Drives for Electric, Hybrid and Fuel Cell Vehicles*, Proceedings of the IEEE, vol.95, no. 4, April 2007.

[16] Wilfred Lewis: *Lewis Formula (Barth Revision)*, Boston Gear catalog, [Tech. Ref. Sheet]. Available: http://viewmold.com/Products/TechnicalReferenceSheet/Gears/Spurgears-lewisformula.pdf; visited, 09.2012

[17] Andrew Novikov, *BMW F1 engines*, All F1 info, [Online]. Available: http://www.allf1.info/engines/bmw.php; visited, 09.2012

[18] Michael J. Fuller, *2006-2008 Audi R10*, Mulsanne's Corner, [Online]. Available: http://www.mulsannescorner.com/audir10-5.html; visited, 09.2012

[19] M. Prummer, J. Auer, A. Schenuwly, *Ultracapacitors drive new efficiencies for hybrid systems architectures.* Maxwell Technologies, Switzerland. [White Paper]. Available: http://www.maxwell.com/products/ultracapacitors/docs/200904_whitepaper_newelectricdriveconcepts.pdf; visited, 09.2012.

[20] Maxwell Technologies: *K2 series ultracapacitors*, [Datasheet]. Available: http://www.maxwell.com/products/ultracapacitors/docs/datasheet_k2_series_1015370.pdf; visited, 09.2012

[21] L. Guzzella, A. Sciarretta, *Vehicle Propulsion Systems*, 2nd ed., Springer, Ed. Berlin, Germany, 2007.

[22] E. Koppen, *Control and Specification of a (Series-Hybrid) Electric Vehicle*, Eindhoven University of Technology, Internship report, 2007.

[23] T. Hofman, *Electric and Hybrid Propulsion Systems*, Eindhoven University of Technology, Lecture notes, 2010.

[24] J. T. B. A. Kessels et al, *Online Energy Management for Hybrid Electric Vehicles*, IEEE Transactions on Vehicular Technology, vol. 57, No. 6, November 2008.

[25] T. Hofman, *Framework for Combined Control and Design Optimization of Hybrid Vehicle Propulsion Systems*, Eindhoven University of Technology, PhD Thesis 2007.

[26] Shell racing fuel: *Diesel LM24*, [Online]. Available: http://shellracing.com.au/shell_diesel_LM24_racing_fuel.html; visited, 09.2012.

[27] Formula 1: *Inside F1/Engine-gearbox*, [Online]. Available: http://www.formula1.com/inside_f1/understanding_the_sport/5280.html; visited, 09.2012.